PHYSICAL REVIEW B VOLUME 21, NUMBER 8 15 APRIL 1980

Magneto-optical studies of PbTe in the far infrared

S. W. McKnight*
Naval Research Laboratory, Washington, D.C. 20375

H. D. Drew
University of Maryland, Department of Physics, College Park, Maryland 20742
(Received 2 October 1979)

Far-infrared magneto-optical studies have been carried out on bulk PbTe with the 10.4- and 3.7-meV lines of a H_2O and an HCN gas laser. Both n- and p-type samples were studied in fields up to 100 kG oriented along the major symmetry axes. Most of the measurements were made in the Voigt geometry. Field modulation permitted high-resolution reflection derivative spectra in which cyclotron resonances, magnetoplasma resonances, and dielectric anomalies were identified by comparison with line shapes predicted from classical magnetoplasma theory in the local limit. In the 10.4-meV data the deviations of the observed line shapes from the classical theory can be interpreted in terms of nonparabolicity of the bands. The observed transitions were fit to a six-band $\vec{k}\cdot\vec{p}$ model, and a set of band parameters was deduced which gave a consistent interpretation of all the 10.4-meV data. The resulting band-edge masses are $m^*(0) = 0.0190 \pm 0.0003$ for n-type and $m^*(0) = 0.0200 \pm 0.0003$ for p-type samples. In the 3.7-meV data, where conditions are far more classical, the line shapes are well represented by a classical calculation but with a mass 15% higher than that predicted by the 10.4-meV data. There is, however, a weak feature in the spectra which corresponds to the lower mass. It is demonstrated that the 15% splitting cannot be interpreted in terms of nonparabolicity or sample inhomogeneities. An interpretation in terms of excitonic modes arising from the phonon-mediated electron-electron interaction is discussed.

I. INTRODUCTION

Because of its interesting physical properties as well as its usefulness in device applications, lead telluride has been studied extensively for more than 25 years using a wide variety of experimental techniques.[1,2] Its small band gap ($E_g \simeq 0.2$ eV) leads to small effective masses and high carrier mobilities. It is a polar semiconductor with a very low-frequency TO phonon giving rise to a very high static dielectric constant $\epsilon_f(0) \simeq 1000$.

In spite of the attention PbTe has received, there has been a surprising disagreement in the literature about some of the basic electronic and lattice parameters. Foley and Langenberg[3] have recently documented the two-order-of-magnitude discrepancy in the static dielectric constant. Measurement of this parameter is complicated by unavoidable effects of the free carriers in PbTe. Experimental determinations of effective masses have also shown a wide spread of values. Historically, some of the difficulty in effective-mass measurements has been due to the dependence of the masses on carrier density, because of the strong nonparabolicity of this narrow-gap semiconductor. While much of the earlier confusion has been removed, recent values[3-5] for the band-bottom mass deviate by as much as 20%.

Some of the discrepancies, particularly in the earlier work, can be attributed to the notorious problems of sample preparation in this soft but brittle material. For example, the carrier concentration is controlled by the stoichiometry, which therefore must be highly uniform. Another complication is that much of the work is on thin films in which the in-plane strains can lead to anamolous properties. The strains can lift the degeneracy of the four carrier pockets leading to unequal occupations.[6] Consequently, because of the nonparabolicity of the bands, effective-mass experiments on thin films must be carefully interpreted.

It must be considered, however, that some of the observed variations in measured properties may be intrinsic to the material and may involve interesting physics. In particular, PbTe is an example of a system of a coupled degenerate electron gas and optically active phonons, and the effects of the electron-phonon interaction in high magnetic fields and degenerate carrier statistics—the conditions of the experiments—are not yet well understood.

Several electron-phonon interaction effects have been observed in PbTe. Saleh and Fan[7] reported the observation of phonon-shifted cyclotron resonance at infrared frequencies, and recent studies of cyclotron resonance near the LO-phonon frequency have shown evidence of mode mixing.[8] Also, a reported composition dependence of the TO-phonon frequency in $Pb_{1-x}Sn_xTe$ alloys has been attributed to renormalization of the phonon through the electron-phonon interaction.[9] We undertook far-infrared magneto-optical studies of bulk PbTe in order to look for electron-phonon interaction effects associated with the cyclotron resonance below the LO-phonon frequency. The polaron mass en-

hancement for PbTe (at zero magnetic field and no free carriers) in only 3%. However, at finite carrier concentration and in the presence of a large quantizing magnetic field, the many-body effects should be severely modified. In the case of the degenerate electron gas in the absence of the electron-phonon interaction, it is known that the magnetic field can produce collective or excitonic modes[10] associated with the inter-sub-band optical transitions, which, in the limit $\hbar\omega_c/E_F \ll 1$, are called Fermi liquid modes.[11] There are also single-particle-like cyclotron-resonance transitions shifted with respect to the collective mode because of mass enhancement. These effects have been studied in bismuth by Verdun and Drew[10] under the conditions of high quantization ($\hbar\omega_c \simeq E_F$). However, the many-body effects in cyclotron resonance in the case of a coupled electron and phonon system under conditions of high quantization have not yet received much attention.[12,13] Consequently the nature of the excitonic modes and mass enhancements are not known for this case.

We have made measurements on the derivative of the reflectance with respect to the magnetic field for n- and p-type samples using far-infrared molecular gas lasers. Both Voigt and Faraday geometries were studied, with emphasis on the former. In the analysis of our data we have discovered several interesting features which have led us to a better understanding of magneto-optical effects in the quantum limit. The observed resonance positions at 119 μm have been fitted to a six-band $\vec{k}\cdot\vec{p}$ model and effective-mass parameters have been obtained. However, these masses appear significantly lower than other recent experimental values. Moreover, our data at 337 μm show two cyclotron-resonance features—a strong feature occurring with a mass close to other reported values and a weaker one that is in agreement with the predictions from our 119-μm data. These observations cannot be understood in terms of band-structure or magnetoplasma effects. An interpretation in terms of many-body effects is advanced and qualitatively discussed.

Previous experiments and the $\vec{k}\cdot\vec{p}$ band-structure models for PbTe are reviewed in Sec. II. In Sec. III we discuss the experimental techniques. The results are presented in Sec. IV, and an analysis of the data in terms of the band models is presented in Sec. V. Section VI is devoted to discussion of the results and the conclusions.

II. BAND-STRUCTURE THEORIES

The problem of accurate effective-mass determination in PbTe has been complicated by uncertainty in earlier work about the proper model to use for the band structure. The early experiments showed that the carriers in PbTe were contained in four nearly ellipsoidal pockets at the L point in the Brillouin zone[14] (Fig. 1). In addition to the conduction and valence bands, split by 187 meV, there are four other nearby bands at the L point (within 2 eV), while all other bands are split off by at least 10 eV.[15] In this situation it has been shown that the band structure can be well represented by $\vec{k}\cdot\vec{p}$ expansion at low carrier concentrations.

The most general dispersion relation for the system that can be obtained from $\vec{k}\cdot\vec{p}$ theory in the absence of an applied magnetic field[16,17] is

$$\left(\frac{\hbar^2k_\perp^2}{2m_t^-}+\frac{\hbar^2k_\parallel^2}{2m_l^-}-\epsilon\right)\left(-E_g-\frac{\hbar^2k_\perp^2}{2m_t^+}-\frac{\hbar^2k_\parallel^2}{2m_l^+}-\epsilon\right)=\frac{\hbar^2}{m^2}(P_\perp^2k_\perp^2+P_\parallel^2k_\parallel^2). \quad (1)$$

Here E_g is the direct gap between the conduction and valence band, and ϵ is the electron energy measured from the bottom of the conduction band. The right-hand side of the equation represents the effect of the interaction between the conduction and valence band, which is treated exactly in this model. P is the velocity matrix element of the $\vec{k}\cdot\vec{p}$ interaction, and the subscripts $\perp$ and $\parallel$ refer to components, respectively, parallel and perpendicular to the [111] axis of the pocket. The terms on the left containing $m_t^\pm$ and $m_l^\pm$ represent the effect of the free-electron mass and the "far bands" (those bands farther from the gap than the conduction and valence bands) as calculated by second-order perturbation theory. Since these bands are split by large energies as compared to E_g, all these terms are expected to be small as compared to E_g or the terms containing P. If all the far-band term terms are set equal to zero, the resulting dispersion relation is the well-known two-band model,[18] which is a fair first approximation in PbTe at low

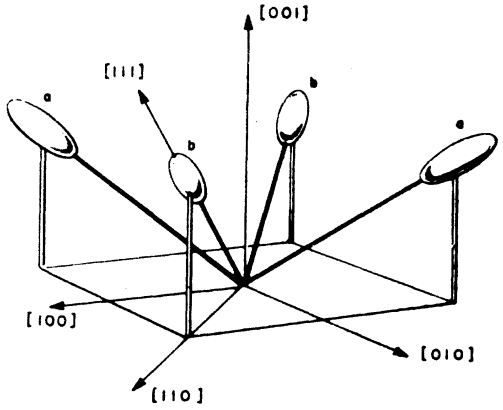

FIG. 1. Fermi surface of PbTe.

carrier concentrations.

In both the two-band and the six-band models the bands are nonparabolic—the effective mass is a function of carrier energy. In the presence of a magnetic field, this implies that the Landau-level spacing differs for transitions between the same levels at different values of momentum along the field k_H. In the quantum limit when there are few Landau levels below the Fermi level, the major contribution to the cyclotron-resonance oscillator strength will come from the transitions near $k_H = 0$, where the joint density of states is large. This means that we need to know only the band energies at $k_H = 0$ to fit resonance positions.

The Hamiltonian for PbTe energy bands in an applied magnetic field has been analyzed by Dimmock.[17] At $k_H = 0$ the Hamiltonian has an analytic solution, but only for the case where the magnetic field is along the [111] symmetry axis of a pocket. To extend the solution to arbitrary orientations of $\vec{H}$, two different approximations have been used. The first approximation, due to the work of Adler, Hewes, and Senturia[19] (AHS), is based on Dimmock's observation[17] that if the condition $m_t^+/m_t^- = P_\parallel^2/P_\perp^2$ holds true, the bands are ellipsoidal, and an exact solution can be found at $k_H = 0$ and any orientation of $\vec{H}$. AHS reasoned that, since the constant-energy surfaces of PbTe are nearly ellipsoidal, it would be a good approximation to use the exact solution but select the values of the parameters to best fit the experimental data without requiring the parameters to hold true to the ellipsoidal ratios. This approximation is exact when $\vec{H}$ is along the [111] axis or when the bands are exactly ellipsoidal. If neither of these conditions hold, it is difficult to determine the accuracy of the approximation. The second approximation is a perturbation approach presented by Dimmock, following the work of Baraff[20] on bismuth. The result, again for any orientation of $\vec{H}$ at $k_H = 0$, is given by Dimmock.[17] This formulation, while never exact, might be expected to be equally valid at any orientation of $\vec{H}$, and it will be more accurate at lower energies.

We have tested these two approximations under conditions appropriate to our experiment—energies calculated for the first three spin-split Landau levels at fields from 10 to 70 kG. In those cases where the AHS approximation is exact—$\vec{H}$ along [111] and for ellipsoidal pockets—we found the Baraff approximation to agree exactly at low energies and deviate by only 1% at the highest energies (100 meV). When the bands were allowed to be nonellipsoidal and $\vec{H}$ was not aligned with the [111] axis, however, this excellent agreement between the two approximations disappeared. In this case, with the AHS model no longer exact, the two models deviated by up to 10% in the predicted energy levels. Since the Baraff approximation was well suited to all cases where exact solutions could be obtained, we interpret these discrepancies to be due to the failure of the AHS model when the ellipsoidal condition breaks down. It appears, therefore, that the Baraff approximation is better suited for the energy and field range in consideration.

The Landau-level structure characteristic of the Dimmock model is shown in Fig. 2. The uneven spacing of the energy levels is a result of the lifting of the degeneracy of the spin-split levels by the far-band terms of the Hamiltonian. Because of this spin splitting, two distinct transitions will be possible for any position of the Fermi level. In general, these transitions will not have the same energy, but a feature of the six-band model when the far-band terms are small is that transitions from levels with the same value of $n+\sigma$ (spin down, $\sigma = 0$; spin up, $\sigma = 1$) have almost exactly the same energy. This fact has important consequences in the interpretation of our measurements.

Experimentally determined band-bottom masses and anisotropies are given in Table I. In addition, we have indicated the band model that was used to extrapolate to the band edge and the type of experiment. ("From literature" indicates that the authors used the results of previous experiments in determing their mass parameters.) As can be seen, there is a wide variation in the band-bottom masses which have been reported, and there is considerable disagreement even among the most recent determinations. These disagreements cannot be attributed to the different models that were used, because in most cases the lowest-carrier-concentration samples that were measured required little extrapolation to the band edge.

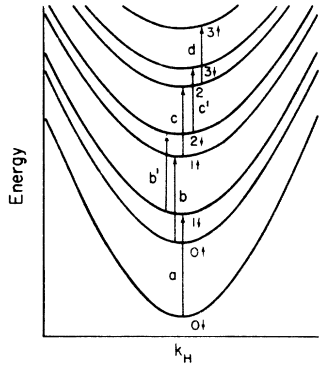

FIG. 2. Landau levels as a function of momentum along the magnetic field from the Dimmock model—showing effects of nonparabolicity and spin-splitting. When the far-band terms are small, transition b is approximately equal to b', c to c', etc.

TABLE I. PbTe band-bottom-mass parameters.

By	Model	Conduction band $m_T(0)$	Conduction band $K(0)$	Valence band $m_T(0)$	Valence band $K(0)$	Experiment
Cuff *et al.* (Ref. 21)	Cohen	0.024 ±0.003	10 ±1.5	0.022 ±0.003	14 ±0.2	Shubnikov–de Haas
Dimmock (Ref. 17)	Dimmock	0.0236	10.1	0.0216	14.1	from literature
Hewes *et al.* (Ref. 22)	Dimmock	0.0242	10.4	0.0251	11.5	Knight shift and literature
Foley and Langenberg (Ref. 3)	Dimmock	0.0164 ± 0.001	9.2 ± 0.3	0.0210 ± 0.0008	11.6 ± 0.2	cyclotron resonance
Ramage *et al.* (Ref. 4)	Two-band			0.026	~11.0	far-ir cyclotron resonance
Burkhard *et al.* (Ref. 5)	Dimmock	0.0222	6.85	0.0242	9.5	far-ir cyclotron resonance

III. EXPERIMENTAL

A. Sample Preparation

Much of the scatter in the experimental results on lead telluride is caused by the difficulty of controlling sample quality. Lead telluride is both soft and brittle. It is very susceptible to surface damage and strain. Striking effects have been observed on thin films due to strain induced by the mismatches of the thermal expansions of the films and their substrates.[6] In bulk samples, surface damage and oxide layers have caused optical properties to change from run to run,[23,24] and because PbTe has a high diffusion coefficient for many materials, contamination can also be a problem.[23] Also, some types of impurities will cause bulk electronic properties to change with time.[3,25] Because of these various problems associated with sample condition, any meaningful experiment with PbTe must involve a great deal of care in sample preparation and characterization.

The PbTe crystals reported on in this paper came from two sources: One sample was grown at the Naval Surface Weapons Center by the Czochralski technique and supplied to us by Burke, and others were prepared by a vapor-growth technique by Schmidt, Bell Labs, and supplied to us by Schmidt and Bishop of the Naval Research Labs. These samples are generally free of the more bizarre effects observed in some crystals used by earlier investigators.[25] We were unable to detect any difference in our results between the samples grown by pulling or by the vapor-growth technique.

Samples were cut from the boules with a diamond string saw, after which the surfaces were oriented and spark planed. The samples were mechanically polished with fine emery cloth and successive grades of alumina polishing compound, down to 0.05-μm grit size. To remove the surface damage caused by mechanical polishing and to prevent possible recrystallization of the surface during annealing, the samples were chemically polished by the method of Schmidt.[26] The samples were then annealed in sealed capsules under 40 Torr of hydrogen gas. Annealing was carried out to guarantee sample homogeneity and to adjust the carrier concentration of the samples. Annealing times and temperatures were taken from the literature.[25,27] After annealing and immediately before inserting in the cryostat, the samples were electropolished by the Norr technique[28] for about 3 min at 10 V. Approximately 30 μm of material were removed by this treatment. We did not mechanically polish the surface after the samples were annealed.

After the far-infrared data were taken, the carrier concentration of the samples was determined by high-field Hall measurements at 4.2 K. The Hall scattering factor[2] was taken equal to 1, and experimental error in the Hall measurements was estimated to be less than 10%. Carrier concentrations and mobilities of the samples reported on are given in Table II along with the temperature at which they were annealed. We found that, while the pulled sample appeared to give good agreement between the equilibrium concentration for the annealing temperature and actual carrier concentration, the vapor-grown samples would approach the equilibrium concentrations only after much longer annealing times. This is in agreement with the observations of Schmidt[29] and is presumably due to the lower density of defects and smaller excesses of the majority component in the vapor-grown samples.

It was possible to test the homogeneity of our samples experimentally. We found that different samples with the same carrier concentrations gave essentially the same spectra. In addition, it was possible to take measurements on the back surface of the samples without removing the sample from the cryostat. These spectra, taken on a surface that had not been electropolished, reproduced all the features of the front surface but were somewhat broadened, as might be expected of a lower quality surface.[30]

TABLE II. Characteristics of experimental samples.

Sample	Type and orientation	Growth	Final anneal T (°C)	Carrier concentration (10^{17} cm^{-3})	Mobility (4.2 K) (10^6 cm^2/V sec)
BU-1 [b]	p type ⟨100⟩	Pulled	302	6.4	0.4 [a]
			235 ± 10	2.3 [a]	0.4 [a]
			235 ± 10	2.7 [a]	0.4 [a]
BI-1 [c]	p type ⟨110⟩	Vapor-grown	230	10	0.2
			407	8.1	
S-1 [d]	p type ⟨110⟩	Vapor-grown	231	5.7	2.0
			230	4.2	2.0
			221	3.5	0.8
			387	21	1.0
BI-2 [c]	p type ⟨110⟩	Vapor-grown	387	17	0.65
S-2 [d]	n type ⟨110⟩	Vapor-grown	407	2.0	1.8
			654	5.2	3.0

[a] Estimate from FIR spectra.
[b] Sample supplied by J. R. Burke.
[c] Sample supplied by S. Bishop.
[d] Sample supplied by P. H. Schmidt.

B. Far-infrared techniques

The experimental configuration is shown in Fig. 3. Far-infrared (fir) radiation for the experiment was provided by two lasers, an HCN laser with strong lasing lines at 337 and 311 μm, and an H_2O-D_2O laser with strong lines at 119 and 171 μm. The samples were mounted in a cryostat in the bore of a 100-kG superconducting magnet and were kept in thermal contact with a 4.2-K helium bath by helium exchange gas. The samples were observed at normal incidence in either the Faraday geometry with the radiation wave vector $\vec{q}$ parallel to the magnetic field, or in the Voigt geometry with $\vec{q} \perp \vec{H}$. The Voigt geometry cryostat had a provision for rotating the sample in place. In this way the spectra could be observed as the angle between the magnetic field and the crystalographic axes was changed. Samples were usually shimmed inside the gear until the magnetic field was within 0.5° of the symmetry plane as determined by x-ray-diffraction measurements. Since the samples are strongly absorbing at these frequencies, all samples were observed in reflection only. The reflected signal was detected by a 4.2-K indium-doped germanium bolometer located in a separate glass Dewar. Copper coils around the sample were used to provide an ac modulation of the magnetic field. Detection at the modulation frequency gave signals that were proportional to the derivative of reflection. Typical modulation fields and frequencies were kept low (~150-G peak to peak at 5 Hz) to minimize signal distortion and eddy current heating. No significant changes in the line shapes were observed on reducing the modulation to as low as 20-G peak to peak. The dramatic effect of this modulation in bringing out features that were hidden in straight reflection is shown in Fig. 4. The line width in a cyclotron-resonance measurement

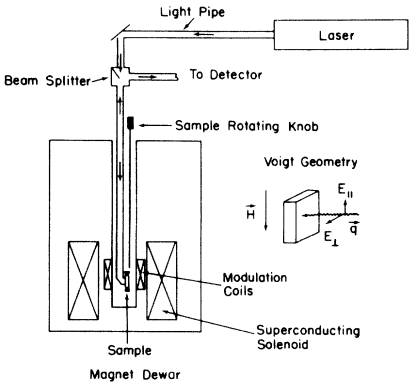

FIG. 3. Experimental configuration. Also shown is the polarization of the electric field vectors of the two modes in the Voigt ($\vec{q} \perp \vec{H}$) geometry.

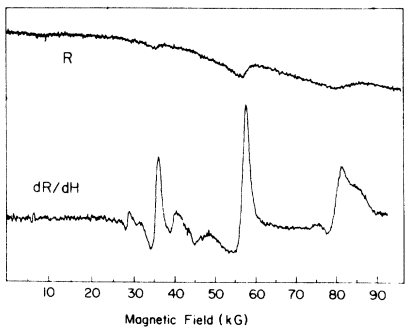

FIG. 4. Signal in straight reflection and derivative in 119 μm of a (110)-plane sample with $\vec{H}$ oriented 23° away from the [111] direction. The zero is offset for the R curve.

is controlled by $\omega\tau$, the product of the radiation frequency and the carrier scattering time. The pronounced features and fine signal-to-noise ratio in this derivative spectrum are a direct result of the high $\omega\tau$ achieved at fir frequencies. The interpretation of these complex spectra require a comparison with the line shapes predicted by magnetoplasma theory.

The dielectric response of a PbTe-like semiconductor in a magnetic field has been calculated using the classical equation-of-motion method by several authors.[31-33] The results are particularly simple in the local limit,[34] where the current is insensitive to the spacial variation of the incident radiation. The real part of the Voigt-geometry dielectric function at 119 μm calculated with parameters typical of PbTe is shown in Fig. 5 as a function of magnetic field along the [110] crystallographic direction. Two distinct cyclotron resonances (CR) are observed because the carrier pockets are not equivalent with this magnetic field orientation. (See Fig. 1.) In addition, a hybrid resonance occurs between the resonance of the high-mass and low-mass electrons. This type of resonance is characteristic of the Voigt geometry with more than one type of carrier and has been discussed in the literature.[31,34] The calculated line shape in dR/dH expected from such a dielectric function is also shown in the figure. The dominating features of the spectrum occur not at the resonances but at slightly higher fields, where the real part of the dielectric function changes signs. The abrupt change in reflectivity when the dielectric function becomes negative and the sample becomes nearly totally reflecting is known as the dielectric anomaly (DA). The DA, not the CR, is usually the dominating feature in the reflectivity spectra, particularly in dR/dH.

The effect of $\omega\tau$ on the spectrum for $\vec{H} \parallel [110]$ is shown in Fig. 6. Note that only in derivative spectra with $\omega\tau > 25$ is the cyclotron-resonance position clearly defined in reflection experiments. For low-frequency (microwave) experiments the cyclotron resonance is not resolved from the accompanying dielectric anomaly and all fits must be made to DA positions. This is a severe disadvantage because DA's are very sensitive to carrier concentration and surface conditions. If an $\omega\tau$ of 50 or greater can be achieved in fir experiments, the actual cyclotron-resonance position can be identified by the small dip preceding the DA feature in dR/dH and the effective masses determined without a difficult fitting procedure.

IV. RESULTS

A. Magnetoreflection at 119 μm

The spectrum obtained at 119 μm on the BU-1 (supplied by Burke) p-type (100)-plane sample ($p \simeq 2.3\times10^{17}$) with $\vec{H}$ along the [110] direction is shown in Fig. 7 along with a best theoretical fit from classical magnetoplasma theory. We note that the experimental trace reproduces the major features of the theory. The CR's at 26 and 76 kG are very sharp and well resolved from the DA, indicating a $\omega\tau$ of 50–100. There are, however, several major discrepancies between the calculated

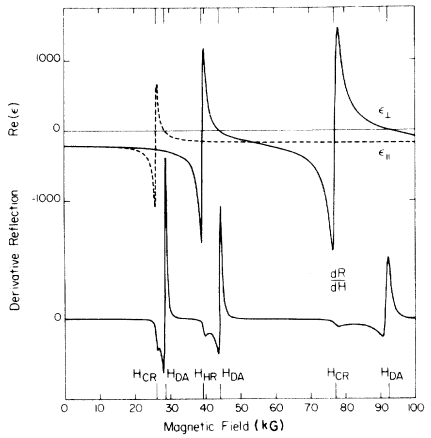

FIG. 5. Real part of the dielectric function versus magnetic field for the two Voigt-geometry modes along with the corresponding calculated signal in derivative reflection. The magnetic field positions of cyclotron resonance, hybrid resonance, and the dielectric anomalies are indicated.

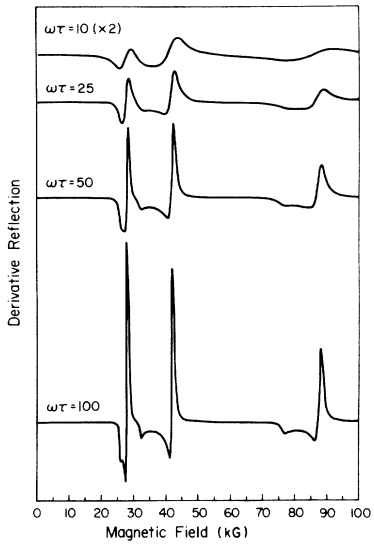

FIG. 6. Calculated spectra for (100)-plane PbTe at 119 μm with $\vec{H} \parallel [110]$, showing the effect of $\omega\tau$ on the spectra.

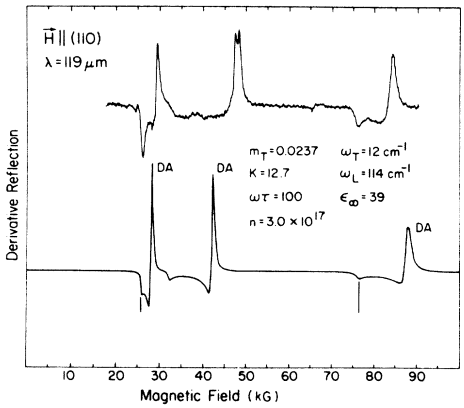

FIG. 7. Experimental trace for the BU-1 sample at 119 μm with $\vec{H} \| [110]$, along with calculation from classical theory with parameters as shown. Carrier concentration of sample is probably about 2.3×10^{17}.

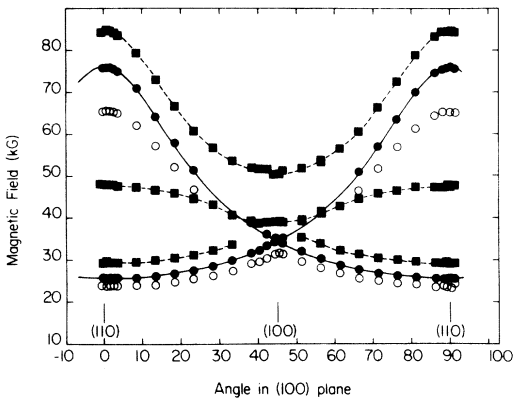

FIG. 8. Angular dependence of magnetic field position of features observed in Voigt geometry on a (100)-plane sample. Squares indicate the dielectric anomalies (the dashed lines have no theoretical significance). Solid circles mark the position of the cyclotron resonances, and the solid line indicates a fit to an ellipsoidal model with m_T and K fixed from data for $\vec{H}$ along [110]. Open circles represent the additional feature discussed in the text.

line shape and experiment:

(1) The position of the DA's is not well fitted by the model. This is not merely an artifact of the values of the parameters chosen. Any adjustment of the parameters that do not affect the CR field positions (i.e., ω_{TO}, ω_{LO}, $\omega\tau$, n, ϵ_∞) will result in theoretical traces in which either all three DA's occur at higher fields than in the illustrated trace, or all three DA's occur at lower fields than shown. The experimental spectrum, on the other hand, has two DA's higher than the theoretical model and one lower. We could find no set of parameters in the local classical model that could fit all the DA positions.

(2) The line shapes in the experimental trace are considerably distorted from the shapes predicted by the theory. The CR's seem to have more relative strength than expected. The negative CR peak is larger rather than smaller than the negative peak of the DA feature. In addition, the hybrid resonance DA at 50 kG appears as a doubled feature. This is not likely to be due to misorientation, because the cyclotron-resonance features exhibited no such splitting.

(3) There is an added feature at 66 kG below the high-field CR and a corresponding feature just below the low-field CR (at about 24 kG). These extra features, which are observed to track with CR as the sample is rotated (Fig. 8), have no counterpart in the local classical theory.

Nonlocal effects can give rise to distortions in line shape and shifts in the resonance position.[34] However, for $\vec{q} \perp \vec{H}$ nonlocal effects depend on $(R_c/\delta)^2$, where δ is the skin depth and R_c is the cyclotron radius, which is generally small at the high fields characteristic of far-infrared experiments.[30,32,34] In this sample, R_c/δ is of order 0.02, so these effects are not due to nonlocality.

We believe these deviations from the theory are a demonstration of the importance of quantum effects in PbTe in this frequency range. Fortunately we are able to directly resolve the cyclotron-resonance features from the DA's, enabling direct determination of effective-mass parameters of the system. Some of the anomalous features of this spectrum will be explained below by quantum effects.

Marking the resonance on the CR feature by reference to the classical theory, we have determined the variation of cyclotron-resonance field with angle as we rotated the sample in the (100) plane. The results are shown in Fig. 8. The solid line in the figure is fit to an ellipsoidal mass:

$$m_c = m_T[K/(K\cos^2\alpha + \sin^2\alpha)]^{1/2},$$

where α is the angle between $\vec{H}$ and the $\langle 111 \rangle$ axis of the pocket. As can be seen, the fit is very good, agreeing to within 2% with experiment. (Uncertainties in marking resonance positions are probably this large.) This is in agreement with other work, which suggests that the Fermi surface of PbTe is very nearly ellipsoidal at low carrier concentrations.[19,35] The values of m_T and K from the fit are $m_T = 0.0237$ and $K = 12.65$. While the value of K is in good agreement with most other measured anisotropies in p-PbTe,[19,35] the value for the mass is somewhat lower than band-bottom masses determined by some authors (see Table I). The discrepancy is larger than indicated by the difference in numbers because for the carrier concentration of this sample the measured mass should be ~10%

higher than the band-bottom mass. This suggests that if only band-structure effects are taken into account, our band-bottom mass is considerably lower than that reported by Hewes *et al.*,[22] Ramage *et al.*,[4] and Burkhart *et al.*[5]

Spectra of the BI-1, BI-2 (supplied by Bishop) and S-1 (supplied by Schmidt) p-type (110)-plane samples over a range of carrier concentrations with $\vec{H} \parallel (110)$ are shown in Fig. 9. The corresponding theoretical spectrum from the classical theory is shown in Fig. 5. Concentrating first on the trace for $p = 3.5 \times 10^{17}$, we can recognize features similar to both the theoretical curve and to the previously discussed spectra of the (100)-plane sample. Cyclotron-resonance features occur at 26 and 76 kG, in the same positions as observed before. We note, as before, distortions in the dielectric anomaly shapes, particularly the anomaly associated with the low-field cyclotron resonance, and excessive strength of the CR features in comparison with the classical line-shape theory. In this spectrum the hybrid resonance itself has a two-peak structure, rather than the hybrid resonance DA as we saw before. The similarity of the spectra for two samples from different sources indicates that the features we see are intrinsic to PbTe.

At the highest carrier concentration, $p = 21 \times 10^{17}$, the spectrum is again similar to the classical theory. We observe a low-field cyclotron resonance shifted up to 29 kG, with some distortion in its accompanying DA, a high-field cyclotron resonance shifted up to 88 kG, with its DA above the highest observable field, and a broad hybrid-resonance DA at 50 kG. The increased effective mass indicated by this spectrum can be explained as due to the band nonparabolicity. Because the Fermi level of this sample is higher than in the low-carrier-concentration samples, the allowed cyclotron transitions originate from a higher Landau level.

At the intermediate carrier concentrations, from 4.2 to 17×10^{17}, the increase in field position of the DA's with carrier concentration is as predicted by the classical theory. Some of the traces, however, show evidence of four cyclotron-resonance features—two at the field positions of the resonances observed for $p = 3.5 \times 10^{17}$ and the other two at the field positions observed at $p = 21 \times 10^{17}$. This behavior, particularly apparent in the spectra for $p = 10$ and 17×10^{17}, indicates two values for m_T and K in the same sample and cannot be explained in terms of classical effects. In a quantum model such behavior would be expected if the Fermi level at $k_H = 0$ lay between two spin-split Landau levels with different transition energies. Similar "two-mass" behavior is observed in these samples with $\vec{H}$ along the [100] and [111] directions. The data for $\vec{H} \parallel [100]$, are shown in Fig. 10, while the $\vec{H} \parallel [111]$ data, which show some unusual quantum effects, will be presented elsewhere.

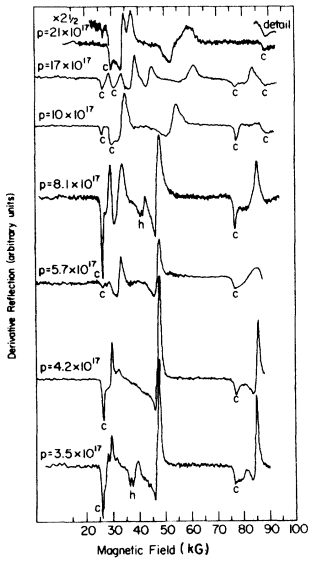

FIG. 9. Spectra for $\vec{H} \parallel [110]$ of p-type (110)-plane samples at 119 μm in Voigt geometry. Resonances labeled c and h are identified with cyclotron resonance and hybrid resonance, respectively. Other features are the associated dielectric anomalies. Carrier concentrations are determined from 4.2-K Hall measurements.

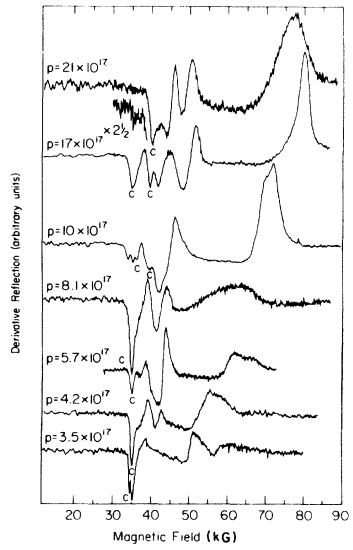

FIG. 10. Spectra for $\vec{H} \parallel [100]$ of p-type (110)-plane samples at 119 μm in Voigt geometry. Features identified with cyclotron resonance are marked with c. The three-peaked structure of the 35-kG CR feature at $p = 10 \times 10^{17}$ is caused by a slight ($\sim 3°$) out-of-the-plane misorientation of this sample.

This mechanism also provides an explanation for the features observed below CR in the (100)-plane sample at very low carrier concentrations (Figs. 7 and 8). It is reasonable to identify the extra resonance with a lower Landau-level transition that becomes allowed when the Fermi level falls below its final state. This interpretation of the extra feature is, in fact, found to be completely consistent with the detailed band analysis in Sec. VI.

The spectra of n-type samples can also be interpreted as showing two different Landau-level transitions. Figure 11 shows the results of experiments at 119 μm on two n-type samples with $\vec{H} \parallel [110]$ in the Voigt geometry. At $n = 2.0 \times 10^{17}$ the spectrum shows characteristics of only one Landau-level transition, leading to cyclotron resonances at about 24 and 64 kG. When the carrier concentration on this sample was raised to 5.6×10^{17} the spectrum is considerably changed. We interpret the spectrum at higher carrier concentration as showing CR features from one Landau-level transition at 24 and 64 kG, as seen at $n = 2.0 \times 10^{17}$, and, in addition, cyclotron-resonance features from a higher Landau-level transition at 27 and 69 kG. The features between 30 and 50 kG are probably hybrid-resonance features that appear split as seen in some p-type samples. The appearance of resonances from two distinct Landau-level transitions in this sample is similar to the behavior found in p-type samples and probably indicates that the Fermi level at resonance lies between two spin-split levels. Data on these n-type samples at other magnetic field orientations is contained in Ref. 30.

The BU-1 sample was run in the Faraday as well as the Voigt geometry. This sample was run as received, with a carrier concentration determined by the grower of 6.4×10^{17}. Contrary to our usual practice, a period of several months had elapsed between the time this sample was electropolished and the time the spectra were obtained. Despite this difference in handling, the spectra in the Voigt geometry closely resembled the spectra obtained on our other samples in this carrier-concentration range. The data in Faraday geometry ($\vec{q} \parallel \vec{H} \parallel [100]$)

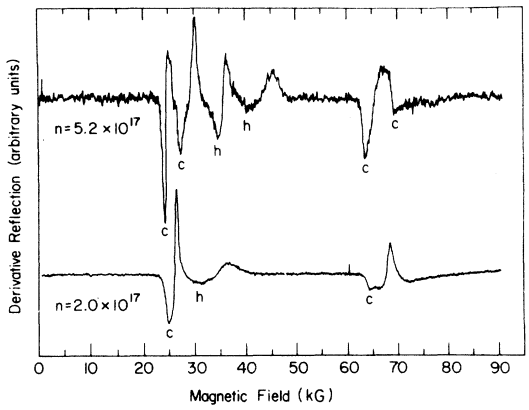

FIG. 11. Spectra for $\vec{H} \parallel [110]$ of n-type (110)-plane samples at 119 μm in Voigt geometry.

showed a resonance feature at 35 kG in the same position as the CR signal observed in Voigt geometry, and a feature at 40 kG corresponding to the second-mass feature discussed before.

When observed in Faraday geometry the cyclotron-resonance signal should be Doppler shifted by nonlocal effects due to the motion of the carriers along the field direction. We have calculated the expected nonlocal shift by the method of Perkowitz.[32] We find that the resonance observed in the Faraday geometry should be shifted upwards by 0.6 kG with respect to the resonance in Voigt geometry where no Doppler shifting is expected. In fact, the cyclotron resonance at 35 kG is observed at the *same* position in Faraday and Voigt geometry. Since the error in marking the resonance position is on the order of 0.2 kG, the Doppler shift should be observable and its absence in the experiment is puzzling.

Table III summarizes the results for n- and p-type samples. The data for each transition at all magnetic field orientations could be fitted within experimental error by an ellipsoidal model, with the given values of transverse effective mass (m_T) and anisotropy (K). Each resonance is identified with a specific Landau-level transition as determined in Sec. VI.

TABLE III. Observed resonances at 118 μm.

Material	Carrier concentration (10^{17} cm^{-3})	Assigned transition	m_T	K
p type	8.1–21	$2\downarrow \rightarrow 3\downarrow$ $(1\uparrow \rightarrow 2\uparrow)$	0.0269 ± 0.0003	13.0 ± 0.2
p type	2.3–17	$1\downarrow \rightarrow 2\downarrow$ $(0\uparrow \rightarrow 1\uparrow)$	0.0237 ± 0.0003	12.7 ± 0.2
p type	2.3	$0\downarrow \rightarrow 1\downarrow$	0.021 ± 0.001	12.5 ± 0.1
n type	5.2	$2\downarrow \rightarrow 3\downarrow$ $(1\uparrow \rightarrow 2\uparrow)$	0.0248 ± 0.0006	9.4 ± 0.5
n type	2.0–5.2	$1\downarrow \rightarrow 2\downarrow$ $(0\uparrow \rightarrow 1\uparrow)$	0.0220 ± 0.0003	10.1 ± 0.2

B. Magnetoreflection at 337 μm

Measurements were made at 337 μm on some of the p-type samples. At this lower frequency cyclotron resonance occurs at lower fields, and $\hbar\omega \ll E_F$. Therefore several Landau levels are below the Fermi level at resonance and the classical approximation should be better than at 119 μm. As shown in Fig. 12, for $\vec{H}$ along [100], the spectrum for this sample with $p = 5.7\times10^{17}$ is well reproduced by a classical calculation with reasonable parameters. Although the high-field DA at 32 kG is broader than predicted, this particular dielectric anomaly is very sensitive to carrier concentration, and a small variation in effective concentration across the sample face would have the effect of broadening the feature.

This DA is also very sensitive to the value of the transverse-optical phonon frequency, so that its position can be used to measure ω_{TO}. If we use the mass at the Fermi level as given by our best fit ($m_T = 0.0268$, $K = 13.0$) we find that $\omega_{TO} = 20$ cm^{-1}. The agreement with Buss and Kinch,[36] who find $\omega_{TO} = 18$ cm^{-1}, is good. Our agreement with Foley and Langenberg,[3] who find $\omega_{TO} = 12$ cm^{-1}, is considerably worse.

Uncertainties in the carrier concentration determined from the Hall measurements, and also in the value chosen for ϵ_∞, will affect the result for ω_{TO}. A 30% decrease in n (or increase in ϵ_∞) will shift the position of the DA down by about 6 kG and bring ω_{TO} into agreement with the Foley-Langenberg value. The value of ϵ_∞ used in these fits (39.0) is the value determined by Lowney,[37] which corresponds to the upper limit of the values considered by Foley and Langenberg, so any adjustment would suggest that ω_{TO} is higher than 18 cm^{-1}. The dependence on the Hall n is the major limiting factor in the accuracy with which we can determine ω_{TO}. We believe that our Hall measurements (allowing for a 10% uncertainty in the Hall scattering factor) are accurate to at least 20%, which makes our results inconsistent with a value as low as 12 cm^{-1}. Some recent work[38] indicates that band bending near the surface of PbTe would have a large effect on the dielectric anomaly positions observed in an experiment such as that of Foley and Langenberg and may explain their unusually low value for ω_{TO}.

Another feature of interest in these 337-μm traces is the small secondary feature observed below CR at about 12 kG in Fig. 12. The feature, which is not predicted in the classical theory, tracks with CR and appears at all orientations of $\vec{H}$ about 15% below the position of cyclotron resonance. Since the nonparabolic mass difference between adjacent Landau levels should be reduced at this lower frequency, it is unclear how the mechanism of spin-split Landau levels which gave 12% splittings at 119 μm could give even larger splittings here. This will be examined quantitatively in the next section with the band-structure model developed from the data at 119 μm.

Misorientation or sample inhomogeneities can be ruled out as a cause of the secondary feature by comparison with 119-μm data. Since the skin depth of the radiation is nearly the same at 119 and 337 μm, inhomogeneous regions or surface effects should affect the spectra at both wavelengths. Figure 13 shows the 337-μm spectrum for $\vec{H} \parallel [110]$ of a sample with $p \simeq 2.7\times10^{17}$, while Fig. 14 shows 119-μm data taken during the same run at the same orientation. While a second feature appears below both the high- and low-field CR at 337 μm, the data at 119 μm is similar to data on other samples and show no splitting in the CR features. This strongly suggests that the secondary feature, which was

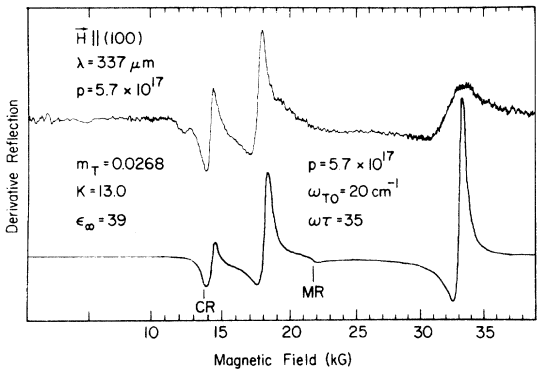

FIG. 12. Spectra for $\vec{H} \parallel [100]$ of a p-type (110)-plane sample at 337 μm in Voigt geometry along with classical calculation with parameters as shown. Calculated position of cyclotron resonance and magnetoplasma resonance are indicated.

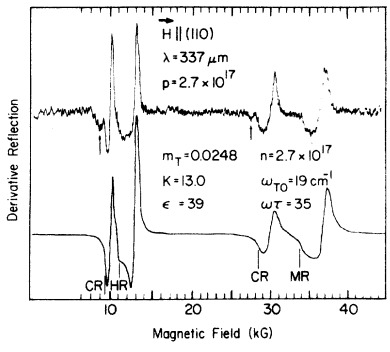

FIG. 13. Spectra for $\vec{H} \parallel [110]$ of a p-type (100)-plane sample at 337 μm in Voigt geometry along with classical calculation with parameters as shown. Positions of cyclotron, hybrid, and magnetoplasma resonances are shown. Arrows indicate the secondary resonance discussed in text.

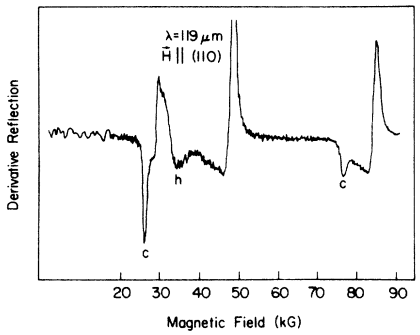

FIG. 14. Data at 119 μm on same sample at same magnetic field orientation as Fig. 13. Cyclotron resonances show no splitting at this frequency, indicating good sample homogeneity.

observed in every sample run at 337 μm, is intrinsic to PbTe. These results at 337 μm are summarized in Table IV.

V. BAND-STRUCTURE ANALYSIS

Cyclotron transition energies in the Dimmock model are completely determined by six effective-mass parameters and the known energy gap. In our experiment at 119 μm we have observed four different cyclotron transitions in n- and p-type PbTe for each of four orientations of the magnetic field, with respect to the axis of the pocket. In addition, one extra resonance was observed at three magnetic field directions for p-PbTe. If we assume that these resonances result from the band structure (i.e., different Landau-level transitions), this gives us a total of 19 independent transition energies which can be used to completely determine (over determine) the effective-mass parameters in PbTe. To carry out this program, however, it is necessary to positively assign the observed resonances to specific Landau-level transitions. Since the resonances appear and disappear as a function of carrier concentration, we assume that they correspond to the Landau transitions at $k_H = 0$ that are allowed by the position of the Fermi level. Only those transitions which have their initial state below the Fermi level and their final state above the Fermi level will be allowed, since PbTe is degenerate and the Fermi surface is sharp at 4.2 K. In this case an unambiguous assignment of resonances to Landau-level transitions can be made in principle by comparing the position of the Fermi level to the position of the Landau levels. There are, however, several difficulties with such an assignment. First, both the Fermi energy and the Landau-level energies are functions of the band parameters, so the assignment must be made self-consistently. Second, the Landau levels (but not the cyclotron-resonance transition energies) are a function of four spin-splitting g factors as well as the effective-mass parameters. Since our experiment is not sensitive to these g factors, values must be obtained where possible from the literature. Third, the Fermi level is not strictly constant as a function of magnetic field. In fact, the Fermi energy undergoes oscillations of a few percent as each Landau level passes through the Fermi level. In addition, when the magnetic field gets so large that only the lowest Landau level is occupied, the Fermi level decreases monotonically as the degeneracy of orbit centers increases with field. Using a two-band model we have estimated the size of this effect in our experiments and find that for $\vec{H} \parallel [110]$ the Fermi level decreases about 10% between 60 kG, when the small mass pockets go into the extreme quantum limit, and 100 kG, which is the limit of our field. This effect is not large compared with other uncertainties in this problem. The larger effects which are seen at higher fields when the small mass pocket becomes depopulated and the large mass pocket goes into the extreme quantum limit are not a factor in our experiment.[5]

Fortunately, because the photon energy ($\hbar\omega$) at 119 μm (10.54 meV) is on the order of the Fermi energy at these concentrations (10–40 meV), there are very few possible Landau-level transitions which can be assigned to the observed resonances. The lowest transition ($0\downarrow$ to $1\downarrow$), which has an energy well separated from any other transition in the Dimmock model, can only be observed at $k_H = 0$ if $E_f < \hbar\omega$ (Fig. 15). From the results of our experiment it is possible to determine approximately where this condition is exceeded. We have seen that at low carrier concentrations the Fermi surface is nearly ellipsoidal. In addition the band-bottom mass $m_T(0)$ must be less than the lowest observed mass. For p-type material we observe

TABLE IV. Observed resonances at 337 μm.

	Lower resonance		Upper resonance	
p (10^{17})	K	m_T	K	m_T
5.7	13.9 ± 0.5	0.0227 ± 0.001	13.0 ± 0.3	0.0263 ± 0.0005
2.7	14.0 ± 0.5	0.0226 ± 0.001	13.0 ± 0.3	0.0248 ± 0.0005
2.3	14.0 ± 0.5	0.0226 ± 0.001	13.0 ± 0.3	0.0248 ± 0.0005

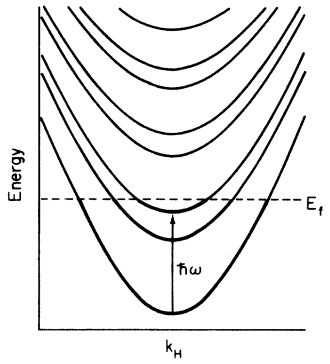

FIG. 15. Lowest Landau-level transition is forbidden at $k_H = 0$ for $\hbar\omega < E_f$.

masses as low as 0.021 and for n-type, 0.022. We also found the anisotropy K to be 12.7 (p-type) and 10.2 (n-type). Assuming a two-band model, the zero-field relation between carrier concentration n and Fermi energy for four ellipsoidal pockets is given by

$$n = \frac{8}{(2\pi)^3}\ \frac{4\pi}{3}\ \sqrt{K}\left|E_f\left(1+\frac{E_f}{E_g}\right)\frac{2m_T(0)}{\hbar^2}\right|^{3/2}. \quad (2)$$

Since $E_f \simeq 10$ meV and E_f/E_g is a small correction, we will take the interaction gap to be equal to the known low-temperature gap (187 meV). The result for the highest carrier concentration at which the lowest transition can be seen for various values of band-bottom masses is shown in Table V. The lowest Landau transition should not be observable in p-type material with p greater than about 2.5×10^{17}, and in n-type material with n greater than about 2.0×10^{17}. With this information it is possible to identify the resonance which was observed only in p-type material with $p \simeq 2.3\times10^{17}$ with the lowest ($0\downarrow \rightarrow 1\downarrow$) transition. The resonance which was observed from $p \simeq 2.3\times10^{17}$ to $p = 17\times \times10^{17}$ must then be the $0\uparrow \rightarrow 1\uparrow$ transition (and $1\downarrow \rightarrow 2\downarrow$, which has nearly the same energy). The third resonance which is seen from $p = 8.1\times10^{17}$ to 21×10^{17} is then the $1\uparrow \rightarrow 2\uparrow$ (and $2\downarrow \rightarrow 3\downarrow$) transition. Similarly, in n-type material the lowest observed resonance, seen at $n = 2.0\times10^{17}$ and 5.2×10^{17}, cannot be the lowest transition but must be identified with the $0\uparrow \rightarrow 1\uparrow$ ($1\downarrow \rightarrow 2\downarrow$) transition. The higher resonance is then the $1\uparrow \rightarrow 2\uparrow$ ($2\downarrow \rightarrow 3\downarrow$) transition. These transition assignments will be shown to be fully self-consistent, while we have been able to find no alternate assignment that is.

TABLE V. Quantum limit carrier concentrations (10^{17} cm^{-3}).

$m_T(0)$	0.016	0.020	0.024
p type			
$p(E_f = h\omega)$	1.5	2.2	2.8
n type			
$n(E_f = h\omega)$	1.4	1.9	2.5

With this identification of the observed resonances, we have carried out a least-squares fit to determine the effective-mass parameters of the Dimmock model. The resonance fields were determined by comparison with classical line-shape calculations in the local limit. Because of the high $\omega\tau$, no large error could be introduced in marking the resonance positions in this way. Theoretical transition energies were calculated using the full magnetic-field-dependent 6-band model of Dimmock with the Baraff-type approximation for magnetic fields not parallel to the (111)-pocket axis. The fitting program converged to nearly identical parameters regardless of the starting values, which were chosen from the literature. A final χ^2 value of 1 (per degree of freedom) corresponded to uncertainties of the order of 0.2%. This is well within the range of our random measurement error without allowance for systematic error due to ignorance of line-shape theory or any possible deviation from the Dimmock model. Therefore we conclude that the experimental agreement with the Dimmock model is excellent. To allow for our uncertainty in judging the resonance positions and other systematic effects, the quoted errors in the final parameter set are calculated including an estimated error of 2% in the resonance position for all except the lowest p-type and highest n-type transitions. These transitions, which were never observed in the absence of other transitions, were judged to be uncertain to within 5%.

The resulting parameters are shown in Table VI along with the results from other authors. The fitting program also returns the errors associated with each parameter and these are also indicated in the table. The wide disparity in these various parameter sets will be discussed in the next section.

The self-consistency of the band-parameter set is indicated in Fig. 16, which shows the magnetic field position of the resonance which is allowed at $k = 0$ by the Fermi level at each carrier concentration. Data with $\vec{H} \parallel [100]$ have been used for convenience. The Fermi level is calculated by numerical integration of the zero-field dispersion relation (Eq. 1) and is assumed to be constant. As discussed previously, this is not a bad assumption for the fields characteristic of our experiment. g factors for n-type material have been determined to be consistent with the experiments of Patel and Slusher.[39] For p-type material there are no comparable experiments from which it is possible to

TABLE VI. Band parameters.

Proposed by	Parameter sets (a.u.) $\frac{\hbar^2 P_{\parallel}^2}{2m}$	$\frac{\hbar^2 P_{\perp}^2}{2m}$	$\frac{\hbar^2}{2m_l^-}$	$\frac{\hbar^2}{2m_t^-}$	$\frac{\hbar^2}{2m_l^+}$	$\frac{\hbar^2}{2m_t^+}$	Derived constants $\frac{2P_{\parallel}^2}{m}$ (eV)	$\frac{2P_{\perp}^2}{m}$ (eV)	$m_T(0)_c$	$m_T(0)_V$	$K(0)_c$	$K(0)_V$
Dimmock	0.033	0.536	1.81	3.38	0.87	7.23	0.45	7.3	0.0236	0.0216	10.1	14.1
Hewes, Adler, and Senturia	0.038	0.41	1.2	11.6	0.7	10.0	0.52	5.6	0.0242	0.0251	10.4	11.5
Foley and Langenberg	0.052	0.599	2.85	17.3	0.353	3.94	0.70	8.2	0.0164	0.0210	9.2	11.6
Burkhardt *et al.*	0.041	0.423	3.57	14.3	1.34	10.5	0.563	5.76	0.0222	0.0242	6.85	9.50
Present work	0.0558 ±0.001	0.555 ±0.005	1.1 ±0.1	12.3 ±0.4	0.0025 ±0.09	9.2 ±0.3	0.76 ±0.01	7.6 ±0.07	0.0190 ±0.0003	0.0202 ±0.0003	10.2 ±0.5	12.2 ±0.6

identify with confidence the exact Landau levels involved in a spin transition. For simplicity we have assumed identical g factors for n- and p-type material, and indicated with the dotted lines the carrier-concentration range in which the resonance could be observed for larger spin splitting.

As can be seen, the n-type data are predicted perfectly by our band model. Within the uncertainties of the g factors and the field dependence of the Fermi level, the p-type data are also consistent with our band-structure model, except for the data at 17×10^{17}. Large changes in the Fermi level or the level energies (~13 meV) would be necessary for this resonance to be allowed in terms of band structure. This resonance may result from inhomogenious regions of the sample, although we had no other experimental evidence that our data were affected by sample quality. Note that for both n- and p-type material the wide ranges of carrier concentration over which resonances are observed is explained as a result of the near degeneracy of transition energies from different spin-split levels (e.g., the transition from $0\uparrow$ to $1\uparrow$ and that from $1\downarrow$ to $2\downarrow$). In summary, the transition assignments that we have made provide a consistent interpretation of nearly all the data at 119 μm. No other assignment gives even fair consistency.

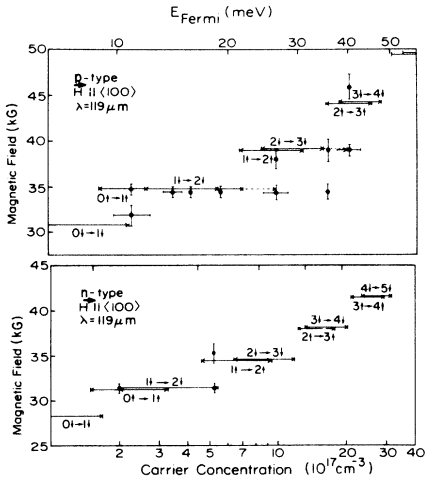

FIG. 16. Magnetic field position of resonances allowed at $k_H=0$ as a function of carrier concentration, calculated with band parameters determined from experiment. Also shown are experimental resonance positions.

VI. DISCUSSION AND CONCLUSIONS

A. Comparison with other band-model parameters and with experiment

Comparing the band parameters derived from our experiment with the parameters found by other authors, we find several interesting discrepancies. First, the band-bottom masses calculated from our model are 10–20% lower than the masses determined by the other authors with the exception of Foley and Langenberg.[3] Since the band parameters of Dimmock[17] and of Hewes, Adler, and Senturia[22] were derived from a wide variety of experiments reported in the literature (with corrections made from the results of Knight-shift experiments by the latter authors), the lower masses predicted in our experiments appear to deviate significantly from the previously accepted values. This deviation can be directly observed comparing Tables III and VI. It is clear that the lowest resonances observed in our experiment are lower than the band-bottom masses determined by Dimmock and Hewes, Adler, and Senturia. The results of Foley and Langenberg, derived from high-frequency microwave CR experiments, are unique in predicting similar or even lower band-bottom masses than those found from our experiment. While their very low value for the n-type mass was determined only after large corrections for nonlocal and nonparabolic ef-

fects, the p-type band-bottom mass (in good agreement with our value) was determined with only small corrections from a low-concentration sample. The parameters of Burkhardt *et al.*[5] are derived from one of several recent experiments on similar "hot-wall" expitaxial films. These films are believed to closely approximate the properties of strain-free bulk PbTe and can thus be compared with our results. Both Burkhard *et al.*[5] and Ramage *et al.*[4] find masses in good agreement with earlier work (10–15% higher than our results), but both find anisotropies lower than generally accepted values. This is particularly evident in the results of Burkhard *et al.* Their parameters give a conduction-band-bottom anisotropy of 6.85, decreasing as the carrier concentration increases. In contrast, most previous experiments found the anisotropy of n-PbTe to be very close to 10. This may suggest that in some way these films are different from bulk samples. For example, strain-induced repopulation effects were found in films by Burke *et al.*[6] Even if this effect were not large enough to completely depopulate pockets, it would, because of band nonparabolicity, increase the mass and decrease the anisotropy observed in a CR experiment.

The effective-mass results of much of the experimental and theoretical work on PbTe are summarized in Fig. 17. The figure does not contain all of the experiments that the theoretical parameter sets were derived from because in some cases (Foley and Langenberg) the results were reported only after extrapolation to the band edge, and in other cases (Hewes *et al.*) use was made of experiments (Knight-shift and interband magneto-optical) which do not give direct values for conduction- or valence-band masses. For p-type material, the results, particularly at higher carrier concentration, lie considerably above the predictions of our model. The good agreement of the model of Foley and Langenberg is partly explained because the results of Burke *et al.* and Jensen *et al.* were included in the data set used by Foley and Langenberg to determine the band parameters. In n-type PbTe the results, primarily from CR-type experiments, are in reasonable agreement and predict an effective mass 10–15% higher than our model predicts. This discrepancy cannot be explained by nonlocal corrections because the experiments of Nii,[40] Fujimoto,[41] and Bishop and Henvis[42] were all done in Voigt geometry where the resonances would be effectively unshifted by nonlocal effects.

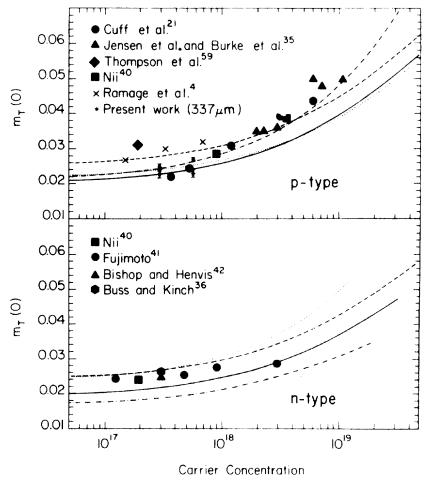

FIG. 17. Transverse effective mass versus carrier concentration for n- and p-type PbTe. Lines are theoretical results from different band-parameter sets: — present work; -- Hewes *et al.*[23]; — • — • — Foley-Langenberg[3]; •••• Dimmock.[17] The symbols represent experimental determinations.

B. Inconsistency of the 337-μm results with the 119-μm band model

The problem posed by the discrepancy between the masses of our band model and other experiments is made even more puzzling by the results of our measurements at 337 μm. As discussed in Sec. IV B, the CR's at 337 μm were split with a secondary feature 15% lower in field than the major CR peak. It was suggested qualitatively that this splitting is too large compared to the splittings at 119 μm to be explained by spin-split Landau levels. This is confirmed by a direct comparison of the data with the predictions of the band model determined from our 119-μm data. Figure 18 shows

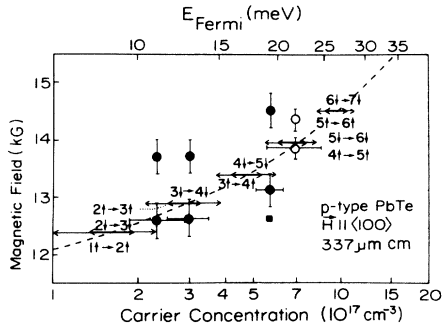

FIG. 18. Observed transitions versus carrier concentration at 337 μm for p-PbTe. Solid circles are transitions observed with $\vec{H}$ along [100] in Voigt geometry. Open circles are resonances observed in Faraday geometry $\vec{H}$ along [100]. Square is resonance position as calculated with ellipsoidal model from data at other symmetry directions. Also shown are the predicted resonance positions from band parameters derived from the 119-μm results: arrows are the allowed Landau-level transitions, and the dashed line is calculated from the zero-field mass at the Fermi level.

the magnetic field position at which resonances would be predicted at 337 μm from our band model, along with the actual data. As can be seen, the splittings observed at 337 μm are more than three times as large as the predicted splittings between adjacent Landau-level transitions. Furthermore, the major (higher-mass) feature of the 337-μm spectra is 8% higher than the band mass predicted by our band model. The smaller secondary feature, on the other hand, is in good agreement with the predictions of the band model. The data at 337 μm cannot, in fact, be described by any reasonable band model. If it is assumed that our band model is incorrect and the effective mass is correctly given by the position of the major peak at 337 μm, then the position of the secondary resonance would correspond to a mass less than the band edge. In this sense, our 337-μm data are similar to the data of Kuchar *et al.*,[43] in which additional features are observed below the position of CR which are inconsistent with band models.

In summary, our data at 119 μm have been compared to classical local magnetoplasma calculations, and features have been identified with cyclotron transitions between different pairs of Landau levels. The transitions corresponding to these resonances have been identified by comparing the position of the Fermi level with the energies of the Landau levels at $k_H = 0$. The resulting band parameters predict Landau-level and Fermi energies that are consistent with our interpretation of the spectra for both n- and p-type samples. Comparison of our band parameters with the parameters proposed by other authors and with experimental results, however, indicates that the effective masses predicted by our band model are 10–20% smaller than those indicated by most previous work. Our data at 337 μm show small features which are consistent with our results at 119 μm and larger features which are in closer agreement with the previous experimental and theoretical work. The splitting between these features at 337 μm is three times too large to be explained by nonparabolicity, and since the spectra at 119 μm of the same samples do not show any unusual features, sample inhomogeneities do not appear to be involved. Similar splittings have been observed in some samples at 337 μm in the experiments of Kuchar *et al.*[43] In the next section we will consider some of the possible interpretations by which such splittings could be explained.

C. Extrinsic effects

Kuchar *et al.*[43] have suggested that their experiments on PbTe can be interpreted in terms of shallow donor states. They base this conclusion on an analysis of the effects of shallow donor states on magneto-optical experiments in nondegenerate semiconductors. Impurity-shifted cyclotron resonance has been observed in high-purity InSb and GaAs, and the theory of these effects is well understood.[44,45] In this case, and in the limit that the donor binding energy is small compared with $\hbar\omega_c$, each Landau level will have a series of bound states lying just below the sub-band edge. The impurity-shifted resonance is a transition where the Landau index and possibly the quantum number of the impurity states are changed. This leads to resonances at lower magnetic fields than the free-carrier cyclotron resonance. However, it is unlikely that PbTe can support such shallow donor states. The major problem is the large static dielectric constant ($\epsilon_0 \cong 1500$) in PbTe which reduces the effective Rydberg ($R^* = e^4 m_{\|}/2\epsilon_0^2\hbar^2$) to 1.2×10^{-6} eV. The binding energy is increased at high magnetic fields as[46]

$$E_B = R^*[2\ln(a_0^*/l_0)]^2 , \quad a_0^*/l_0 \gg 1$$

where a_0^* is the effective Bohr radius

$$a_0^* \equiv \epsilon_0\hbar^2/m_{\|}e^2 \approx 0.4 \ \mu\text{m} ,$$

and $l_0 = (\hbar c/eB)^{1/2}$ is the magnetic length.

In degenerate semiconductors the binding will be reduced because of the screening of the impurity potential by the free carriers. Even if this screening is ignored, the binding energy is only estimated to be $E_B \approx 0.08$ meV. To explain the magneto-optical experiments, however, a binding energy larger than 1 meV is required. Therefore we feel that it is highly unlikely that these experiments can be interpreted in terms of shallow impurity levels.

Another possible interpretation of both experiments is in terms of surface-space charge layers. Schaber *et al.*[38] find extra resonances in the Faraday geometry when an electric field is applied normal to the surface of PbTe thin films. The simplest idea is to consider the surface density different than the bulk due to accumulation or depletion of carriers. Since we assume we have observed all three of the lowest transitions in p-type PbTe this density effect could only lead to an even lower band-edge mass. At the carrier concentrations of our samples the region of band bending is confined much closer to the surface than was the case for the Schaber *et al.* experiments. We estimate the thickness of an accumulation or depletion layer on our samples to be of the order of 500 Å. Since the penetration depth of the far-infrared radiation is typically greater than 2000 Å even at resonance, it is hard to imagine that surface resonances would dominate the cyclotron-resonance signals. We also note that in our Voigt-geometry experiments the surface levels are mixed magnetic and electric po-

tential surface states which have a spread-out density of states[47] in comparison to the case of the Faraday-geometry experiments of Schaber *et al.* Therefore the surface-resonance features should be broadened in comparison with the bulk resonance.

Since we obtain consistent results for different samples and different surface preparations, which are likely to change the band bending at the surface, we believe our cyclotron-resonance peaks are associated with bulk cyclotron resonance. However, experiments on space-charge layers in bulk PbTe in the Voigt geometry would test this conclusion.

D. Many-body effects

PbTe is an example of a system with a coupled degenerate electron gas and polar optical phonons. Consequently the possibility of interpretations in terms of many-body interactions should not be overlooked. Under the conditions of these magneto-optical experiments, the cyclotron frequency (ω_c), the LO phonon frequency (ω_{LO}), and the plasma frequency (ω_p) are all comparable so that the interaction effects are complicated, and they can be quite large as we shall see. We can consider several many-body effects that could affect the cyclotron-resonance measurements: (1) the mass enhancement or self-energy effects familiar in the polaron problem, (2) plasmon-or phonon-assisted cyclotron resonance wherein the Landau-level transitions are accompanied by the emission (or absorption at finite temperature) of a phonon or plasmon, and (3) finally there is the possibility of final-state interaction effects such as occur in the case of excitons.

1. Self-energy effects

In an empty polar lattice a single electron near the band edge polarizes the lattice, and this electron plus lattice polarization produces an enhanced effective mass m^*. This is the polaron problem which has a wide literature.[48] The result for an electron at the band edge is

$$m^* = m_b(1+\alpha/6),$$

where m_b is the band mass and α is the polaron coupling constant

$$\alpha = \frac{e^2}{\hbar}\left(\frac{m^*}{2\hbar\omega\,\omega_{LO}}\right)^{1/2}\left(\frac{1}{\epsilon_\infty}-\frac{1}{\epsilon_0}\right).$$

For PbTe, $\alpha \approx 0.15$, which produces a mass enhancement of only 2.5%. This result is not applicable to our experiments since the electron-phonon interaction is modified by screening effects and Pauli-principle restriction at the carrier densities of our samples. This problem has been considered in the $H=0$ case, and it becomes identical to the metallic case with an Einstein phonon spectrum.[12] We have estimated the mass enhancement for our samples from this theory and find $m^*/m_b \approx 1.03$—still too small to account for the experiments.

However, these theories do not include the effects of the quantization of the electronic spectrum in a strong magnetic field. The magnetic field introduces two important modifications of the system. First, additional longitudinal magnetoplasma modes are introduced, which could produce an extra contribtuion to the mass enhancement in comparison with the $H=0$ case. In addition, for a highly quantized system ($\hbar\omega_c \simeq \epsilon_F$), the electron density of states is strongly modified with inverse-square-root singularities for energies near the bottoms of the Landau levels. These singularities in the density of states can produce a corresponding large effect on the electron self-energies.

The electron self-energies in the degenerate electron gas can be treated by considering the electron-electron interaction screened by the total dielectric function of the system $\epsilon(q,\omega)$:

$$\epsilon(q,\omega) = \epsilon_e(q,\omega) + \epsilon_l(\omega),$$

where $\epsilon_e(q,\omega)$ is the dielectric function for the electron which is adequately given for this problem by the random-phase approximation. For $H=0$, ϵ_e would be the Lindhard function, but for $H\neq 0$ it becomes much more complicated.[49] $\epsilon_l(\omega)$ is the lattice contribution which for a polar semiconductor is given by

$$\epsilon_l(\omega) = \epsilon_\infty \frac{\omega_{LO}^2-\omega^2}{\omega_{TO}^2-\omega^2}.$$

From this form of $\epsilon(q,\omega)$, we see that the effective electron-electron interaction is dynamically screened corresponding to a retarded interaction. This is similar to the interaction that gives rise to superconductivity in metals. Because ϵ_l for PbTe is usually large [$\epsilon_l(0)\cong 1500$], the effective interaction potential $V_{eff} = V(q)/\epsilon(q,\omega)$ is small except near the zeros of ϵ. These zeros correspond to the longitudinal mixed magnetoplasma and phonon modes of the system and the problem can be recast in terms of the electron-plasmon interaction by using the plasmon pole approximation. At long wavelengths the plasmons are given by the roots Ω of[50]

$$\epsilon(0,\Omega) = \epsilon_\infty\left(\frac{\omega_{LO}^2-\Omega^2}{\omega_{TO}^2-\Omega^2}\right) - \frac{\omega_p^2\sin^2\theta}{\Omega^2-\omega_c^2} - \frac{\omega_p^2\cos^2\theta}{\Omega^2} = 0,$$

where θ is the angle between the magnetic field and the plasmon wave vector. The dispersion relation for these modes are shown schematically for the case of PbTe with $\vec{H} \parallel [100]$ in Fig. 19.

The simplest contribution to the single-particle

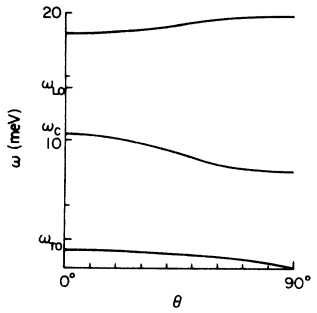

FIG. 19. Dispersion of magnetoplasma modes in the low-$\vec{q}$ limit for PbTe with $\vec{H} \| [100]$. The carrier density is $4 \times 10^{17}/\mathrm{cm}^{-3}$. θ is the angle between $\vec{q}$ and $\vec{H}$.

self-energies Σ is given by the exchange term in the Hartree-Fock approximation

$$\Sigma(n, k_y, k_z) = -\sum_{n', k_z', k_y'} \frac{\langle n, k_z, k_y | V(q) | n', k_z', k_y' \rangle}{\epsilon(q, \omega)} f(n', k_z'),$$

where f is the Fermi occupation factor, $\vec{q} = \vec{k} - \vec{k}'$, $\omega = [E(n,k) - E(n',k')]/\hbar$, and $E(n,k)$ is the single-particle dispersion law in the absence of the electron-electron interactions. In the absence of final-state-interaction effects or finite-lifetime effects, the transitions energies ΔE in the cyclotron-resonance experiments will depend on k and will be given by

$$\Delta E(k) = E(n+1, k_z, k_y) + \Sigma(n+1, k_z, k_y) - E(n, k_z, k_y) - \Sigma(n, k_z, k_y).$$

Because of the inverse-square-root singularities in the density of states associated with the bottom of the Landau sub-bands, it is possible to get large self-energy effects. In particular, if $E_n(k) - E_{n'}(0) \approx \hbar\Omega_i$, where $\Omega_i(k)$ is a root of $\epsilon(k, \Omega_i) = 0$, $\Sigma(n,k)$ will be singular (in the absence of damping). This is due to the resonant exchange interaction with those electrons in the large phase space near $k_H = 0$. These effects can be much larger than the polaron mass enhancement referred to above. Indeed preliminary self-energy calculations for PbTe using an approximate $\epsilon_e(q, \omega)$ indicate a spread in the resonance energies for cyclotron resonance of the right magnitude to account for the difference between our 337- and 119-μm data or the mass discrepancies in the literature.[51]

It does not seem likely, however, that all the experimental results can be accounted for by self-energy effects alone. For example, in our experiments it remains to be explained why the oscillator strength in the 119-μm spectrum is large for low m^* and that of 337 μm is large for a higher m^*. When the results of Foley and Langenberg are also considered, it appears that the mass may oscillate with frequency. (These microwave experiments give an m^* somewhat lower than our 119-μm measurements.) The experiments of Kuchar *et al.* suggest two or three isolated peaks in the oscillator strength associated with the cyclotron resonance, and the strong temperature dependence they observed must be explained (assuming that their results are also related to many-body effects). The significance of the self-energy calculation is that it indicates that the electron-electron interaction effects are at least large enough to be responsible for the m^* anomalies that have been observed in the magneto-optical experiments on PbTe.

2. *Plasmon emission*

The plasmon-emission process is closely related to the LO-phonon-shifted cyclotron resonance that has been observed in several experiments in different materials. We have noted that this effect has been observed at high frequency in PbTe by Saleh and Fan.[7] Plasmon-emission effects have been observed in the degenerate electron gas by McCombe *et al.*[52] in n-type InSb. (These experiments were done under conditions $\omega \gg \omega_p$ and the extreme quantum limit.) They have observed absorption in the inactive mode near the condition for cyclotron resonance and the harmonics. The fundamental absorption peak occurs near $\omega = (\omega_c^2 + \omega_p^2)^{1/2}$ and shifts accordingly with carrier concentration. This absorption line has been interpreted in terms of a process in which the incident photon creates an electron-hole pair plus a plasmon. In the final state both the electron and hole are in the $n = 0$ Landau level so that the excitation energy is $\hbar\omega = \hbar\Omega^+ + E(k_e) - E(k_h)$, where Ω^+ is the plasmon frequency, $E(k)$ is the band energy, and $E(k_e) - E(k_h) \lesssim E_F \ll \hbar\omega_c$. The plasma modes in the long-wavelength limit in this case are the roots Ω^+ of $\epsilon_l(0) + \epsilon_e(\omega) = 0$, since the frequency ω is much lower than the TO-phonon frequency.

Golden-rule calculations of the line shapes considering the above process produce absorption peaks in the correct positions. The calculation shows that most of the absorption comes from emission of $\theta \approx 90°$ plasmons in the high-frequency plasmon branch. This theory is not complete, however, as other processes which are required for a current-conserving approximation[53,54] have been ignored. When these terms are included it has been shown that there is only absorption at $\omega = \omega_c$ in the active mode as demanded by the Kohn theorem.[55] To account for the violation of the Kohn theorem in these experiments, it has been necessary to invoke the breaking of the translational in-

variance by the presence of impurities.[56] However, at present there is no quantitative line-shape theory for these experiments that includes the impurity effects.

In the far-infrared experiments on PbTe we could expect absorption when $\hbar\omega = E(n,k) - E(n',k-q) + \hbar\Omega_i(q)$ where the first term on the right-hand side is the final state of the electron, the second term its initial state, and $\Omega_i(q)$ is a magnetoplasmon. $\Delta E = E(n,k) - E(n',k-q) \geq 0$ so that the high-frequency branch ($\Omega > \omega$) cannot be involved in our experiments. Since we are observing ~20% mass shifts, we must have

$$\Delta\epsilon + \hbar\Omega_i(q) \approx \hbar\omega_c .$$

For the low-frequency branch $\Omega_1 \ll \omega_c$ near resonance at 119 μm (see Fig. 19). If we take $\Delta\epsilon \approx \hbar\omega_c$ as expected from a density-of-states argument, we would expect a mass $\Omega_1/\omega_c \sim 0.15$ lower than the band mass from this mode. However, this same process would produce a 40% apparent mass reduction at 337 μm contrary to observation. Moreover, the coupling constant[50] for this branch, $D(q) = (4\pi e^2/q^2)(\partial\epsilon/\partial\omega)^{-1}_{\Omega_1}$, is very small in comparison with other plasmon branches.

For the center branch (Fig. 19) $\Omega \simeq \hbar\omega_c$, which would require $\Delta\epsilon \ll \hbar\omega_c$. If we assume $\Delta\epsilon = 0$ we find that the resonance is shifted in the wrong direction to account for the low masses observed in our experiments. We can find no argument that would support an interpretation in terms of plasmon emission involving this plasmon branch.

3. *Final-state interactions*

Finally we will consider the effects of final-state interactions in the resonance. In the resonant transition the excited (inter-Landau level) electron-hole pair can interact via the screened Coulomb interaction and possibly set up an excitonlike collective state shifted with respect to the usual cyclotron resonance. These effects have been observed in far-infrared cyclotron-resonance experiments on bismuth.[10,57]

The line shapes of the CR transitions characteristically contained fine structure with a sharp feature on the high-field side of the resonance. It was found that these sharp features could be interpreted in terms of excitonlike modes associated with the inter-sub-band transition.[10]

Verdun developed a theory of these excitonic modes and the optical conductivity of the system within the generalized random-phase approximation (RPA). Under conditions where the interaction between electrons can be taken as statically screened ($\omega \ll \omega_p$) the generalized RPA is consistent with current conservation and so the theory obeys the Kohn theorem requirement that the only excitation observable in an isotropic electronic system at $q = 0$ occurs[55] at $\omega = \omega_c$.

Schematic excitation spectra from this theory are shown in Fig. 20. The modes in the continuum are raised in comparison with the noninteracting case by self-energy effects (the exchange interaction). There are typically several collective or excitonic modes split off from the continuum. For an isotropic system the ground excitonic level lies precisely at ω_c when $q = 0$. Moreover, all the oscillator strength is in this principle mode, thus satisfying the Kohn theorem.[55] These excitonic modes are in fact the microscopic equivalent of the Fermi-liquid modes in Landau theory,[11] and Verdun's theory is the correct microscopic theory for $r_s \ll 1$ and static screening ($\omega \ll \omega_p$). (r_s is the Fermi-liquid parameter which characterizes the strength of the electron-electron interaction.)

Verdun's theory successfully accounted for a large set of experimentally observed absorption line shapes for cyclotron resonance and harmonics, spin flip, and combined resonances in bismuth.[58] These results indicate that the case of weak electron-electron interaction ($r_s \ll 1$) and static screening ($\omega \ll \omega_p$) are well understood.

In applying these ideas to the case of PbTe experiments, there are several important differences that must be considered. First, the effective interaction has both attractive and repulsive characteristics depending on the frequency at which the

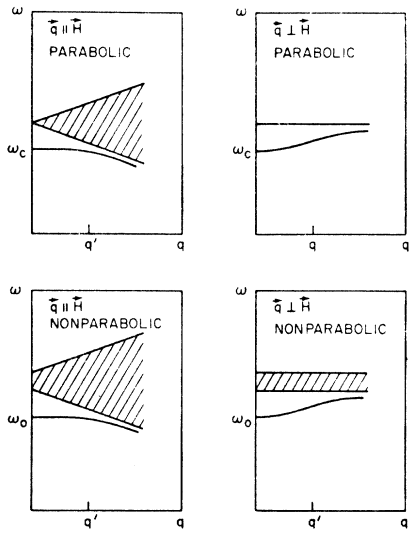

FIG. 20. Schematic excitation spectrum for a degenerate electron system with parabolic and nonparabolic energy bands. The shaded area represents a continuum of excitation, and the solid line represents an excitonlike collective mode. Depending on the interaction potential the exciton modes can lie below or above the continuum.

dielectric constant is evaluated. This indicates the possibility of exciton modes both above and below the continuum modes. A second point is that the interaction is retarded or frequency dependent. Consequently Verdun's theory is no longer valid and terms beyond the RPA must be included for a current-conserving theory.[53]

This problem has been extensively discussed in the literature in connection with the plasmon-shifted cyclotron-resonance experiments in n-type InSb by McCombe *et al.*[54,56] Owing to the complicated nature of the additional terms in the theory, there have been no quantitative calculations of the conductivity for the case of a dynamically screened interaction. In the absence of a theory, we can only speculate on whether such excitonic features could be involved in the PbTe experiments. The data of Kuchar *et al.* are strongly suggestive of excitons. In particular, their 195-μm data could be interpreted in terms of two excitonlike modes on the low-field side of the ordinary single-particle-like cyclotron-resonance feature. Also, in our data a similar excitonic description would possibly explain the discrepancies between our 337- and 119-μm data and the differences in our masses and those reported in the literature. First we would interpret the weak low-field structure in the 337-μm data as an excitonic mode and the high-field feature as the single-particle cyclotron resonance. Then at 119 μm we conjecture that the exciton mode on the low-field side of the resonance has a large oscillator strength so that the continuum mode is lost in the dielectric anomaly structure. This interpretation goes a long way toward reconciling the discrepancies in the reported cyclotron masses. In addition, the apparent lack of Doppler shifting in our Faraday results at 119 μm is explained by this interpretation. The dispersion of the collective mode is quadratic ($\propto q^2$) for small q. For the small wave vectors of our experiment the collective mode could be essentially unshifted compared with the linear shift dispersion ($\propto qV_F/\omega_c$) calculated for the single-particle mode. As a result the resonance would occur at the same field in the Voigt and Faraday geometry—as observed.

We note that the situation in the microwave measurements may be quite different than that for the far-infrared experiments. The cyclotron frequency is lower than ω_{TO} and so the plasma modes are quite different. Also, the field is lower so that the mass enhancement may be closer to the $H=0$ case discussed earlier. Therefore we suggest their results can be understood in terms of a small mass enhancement and the absence of excitons (possibly due to $\omega\tau$ effects).

Finally there is the question of how to interpret the band parameter derived from our 119-μm data. First we note the remarkable consistency of the data with the $\vec{k}\cdot\vec{P}$ band model for four different samples with carrier concentrations varying between 2×10^{17} and $2\times10^{18}/\mathrm{cm}^3$. We suggest that our measured masses may in fact be quite close to the bare-band masses. It is likely that the electron-electron interaction gives rise to a large mass enhancement due to the self-energy effects, but then the collective or excitonlike mode essentially cancels this shift so that the exciton mode falls at the position corresponding to the bare-band mass. This is precisely what happens in the isotropic electron gas as is required by the Kohn theorem.

In conclusion, we believe there is a strong possibility that the explanation of much of the remarkable discrepancies reported for the cyclotron mass in PbTe is to be understood in terms of many-body effects. It may also be possible that the $\vec{k}\cdot\vec{P}$ band parameters derived from our 119-μm data may represent essentially the bare-band parameters in the absence of many-body effects. There is a need for a better theoretical treatment of the coupled electron-phonon system before these ideas can be confirmed.

Note added. The g factors in PbTe have recently been measured by two different magneto-optical experiments. Schaber and Doezema [Solid State Commun. 31, 197 (1979)] have measured the spin resonance in low-carrier-concentration epitaxial films. A complete set of band parameters has been deduced from interband magneto-optical measurements by Appold, Grisar, Bauer, Burkhard, Ebert, Pascher, and Hafele [*Proceedings of the 14th International Conference on the Physics of Semiconductors, Edinburgh*, edited by B. L. H. Wilson (Institute of Physics, London, 1979), p. 1101].

ACKNOWLEDGMENTS

The authors would like to thank J. R. Burke, P. H. Schmidt, S. Bishop, and S. Groves for supplying samples for this experiment, and for advice on sample preparation. Useful discussions with E. Yorke, A. Bardasis, H. Verdun, and J. Lowney are gratefully acknowledged. One of the authors (S.W.M.) would like to express his appreciation to Dr. S. Perkowitz and the faculty and staff at Emory University where much of this work was completed. Research was supported by the NSF under Grant No. DMR-77-28399-A01.

*NRC-NRL resident research associate.
[1]See the review article by R. Dalven, Infrared Phys. 9, 141 (1969).
[2]Yu. I. Ravich, B. A. Efimova, and I. A. Smirnov, *Semiconducting Lead Chalcogenides* (Plenum, New York, 1970).
[3]G. M. T. Foley and D. N. Langenberg, Phys. Rev. B 15, 4830 (1977).
[4]J. C. Ramage, F. Kuchar, R. A. Stradling, and A. Lopez-Otero, J. Phys. C 10, 5089 (1977).
[5]H. Burkhard, G. Bauer, and W. Zawadzki, Phys. Rev. B 19, 5149 (1979).
[6]J. R. Burke and G. P. Carver, Phys. Rev. B 17, 2719 (1978).
[7]A. S. Salih and H. Y. Fan, Phys. Rev. B 5, 3972 (1972).
[8]H. Burkhard, G. Bauer, P. Grosse, and A. Lopez-Otero, Phys. Status Solidi B 76, 259 (1976).
[9]H. Kawamura, S. Katayama, S. Takano and S. Hotta, Solid State Commun. 14, 259 (1974).
[10]H. D. Drew and H. R. Verdun, Phys. Cond. Matter 19, 371 (1975); H. R. Verdun and H. D. Drew, Phys. Rev. B 15, 5636 (1977).
[11]P. M. Platzman and P. A. Wolff, *Waves and Interactions in Solid State Plasmas* (Academic, New York, 1973).
[12]Degenerate semiconductors in zero magnetic field have been considered by G. D. Mahan, in *Polarons in Ionic Crystals and Polar Semiconductors*, edited by J. T. Devreese (North-Holland, Amsterdam, 1972), pp. 553–657.
[13]P. Vogl, in *Physics of Narrow Gap Semiconductors*, edited by J. Rouxuszkiewicz, M. Gorska, and E. Kaczmarek (PWN-Polish Scientific Publishers, Warsaw, 1978), p. 131.
[14]K. F. Cuff, M. R. Ellett and C. D. Kuglin, *Proceedings of International Conference on the Physics of Semiconductors, Exeter, England, 1962* (The Physical Society, London, 1962).
[15]P. J. Lin and L. Kleinman, Phys. Rev. 142, 478 (1966); G. Martinez, M. Schluter and M. L. Cohen, Phys. Rev. B 11, 651 (1975).
[16]D. L. Mitchell and R. F. Wallis, Phys. Rev. 151, 581 (1966).
[17]J. O. Dimmock, in *The Physics of Semimetals and Narrow Gap Semiconductors*, edited by D. L. Carter and R. T. Bate (Pergamon, New York, 1971).
[18]B. Lax, J. G. Mavroides, H. J. Zeiger, and R. J. Keyes, Phys. Rev. Lett. 5, 241 (1960).
[19]M. S. Adler, C. R. Hewes, and S. D. Senturia, Phys. Rev. B 7, 5186 (1973).
[20]G. A. Baraff, Phys. Rev. 137, A842 (1965).
[21]K. F. Cuff, M. R. Ellett, C. D. Kuglin, and L. R. Williams, *Physics of Semiconductors: Proceedings of the Seventh International Conference*, Paris, 1964 (Academic, New York, 1964).
[22]C. R. Hewes, M. S. Adler, and S. D. Senturia, Phys. Rev. B 7, 5195 (1973).
[23]G. M. T. Foley, Ph.D. thesis, University of Pennsylvania, 1975 (unpublished).
[24]S. Perkowitz, Phys. Rev. B 12, 3210 (1975).
[25]R. F. Brebrick and R. S. Allgaier, J. Chem. Phys. 32, 1826 (1960); R. F. Brebrick and E. Gubner, *ibid.* 36, 1283 (1962).
[26]P. H. Schmidt, J. Electrochem. Soc. 109, (1962).
[27]W. W. Scanlon, Phys. Rev. 126, 509 (1962).
[28]M. K. Norr, J. Electrochem. Soc. 109, 433 (1962).
[29]P. Schmidt, private communication.
[30]S. McKnight, Ph.D. thesis University of Maryland, 1977 (unpublished).
[31]H. Numata and Y. Uemura, J. Phys. Soc. Jpn. 19 2140 (1964).
[32]S. Perkowitz, Phys. Rev. 182, 828 (1969); Ph.D. thesis, University of Pennsylvania, 1966 (unpublished).
[33]P. R. Wallace, K. K. Chandler, and J. Harnad, Can. J. Phys. 46, 243 (1968).
[34]A review of work on magnetoplasma theory and an extensive list of references is contained in E. D. Palik and J. K. Furdyna, Rep. Prog. Phys. 33, 1193 (1970).
[35]J. R. Burke, B. Houston, and H. T. Savage, Phys. Rev. B 2, 1977 (1970). J. D. Jensen, B. Houston, and J. R. Burke, *ibid.* 18, 5567 (1978).
[36]D. D. Buss and M. A. Kinch, in *Proceedings of the Conference on the Physics of IV-VI Compounds and Alloys*, edited by S. Rabii (Gordon and Breach, New York, 1974), p. 209.
[37]J. Lowney, Ph.D. thesis MIT, 1975 (unpublished).
[38]H. Schaber, R. E. Doezema, and J. F. Koch, Solid State Commun. 27, 7 (1978).
[39]C. K. N. Patel and R. E. Slusher, Phys. Rev. 177, 1200 (1969).
[40]Riro Nii, J. Phys. Soc. Jpn. 19, 58 (1964).
[41]M. Fujimoto, J. Phys. Soc. Jpn. 21, 1704 (1966).
[42]S. G. Bishop and B. W. Henvis, Solid State Commun. 7, 437 (1969).
[43]F. Kuchar, J. C. Ramage, R. A. Stradling, and A. Lopez-Otero, J. Phys. C 10, 5101 (1977).
[44]R. Kaplan, Phys. Rev. 181, 1154 (1969).
[45]H. R. Fetterman, D. M. Larsen, G. E. Stillman, P. E. Tannenwald, and J. Waldman, Phys. Rev. Lett. 26, 975 (1971).
[46]R. Cohen, J. Lodenquai, and M. Ruderman, Phys. Rev. Lett. 25, 407 (1970).
[47]W. Beinvogl, Avid Kamgar, and J. F. Koch, Phys. Rev. B 10, 4274 (1976).
[48]See for example, C. Kittel, *Quantum Theory of Solids* (Wiley, New York, 1963), Chap. 7.
[49]N. J. Horing, Ann. Phys. (N.Y.) 31, 1 (1965).
[50]V. Celli and N. D. Mermin, Ann. Phys. (N.Y.) 30, 249 (1964).
[51]A. Bardasis and E. Yorke, unpublished.
[52]B. D. McCombe, R. J. Wagner, S. Teitler, and J. J. Quinn, Phys. Rev. Lett. 28, 37 (1972).
[53]M. Watabe, J. Phys. Soc. Jpn. 28, 655 (1970).
[54]C. S. Ting, S. C. Ying, and J. J. Quinn, in *Proceedings of the Thirteenth International Conference on the Physics of Semiconductors, Rome*, edited by F. G. Fumi (North-Holland, Amsterdam, 1976), p. 1008.
[55]W. Kohn, Phys. Rev. 123, 1242 (1961).
[56]J. J. Quinn, B. D. McCombe, K. L. Ngai, and T. L. Reinecke, Phys. Letters 54A, 101 (1975).
[57]H. R. Verdun and H. D. Drew, Phys. Rev. Lett. 33, 1608 (1974).
[58]H. R. Verdun and H. D. Drew, Phys. Rev. B 14, 1370 (1976).
[59]T. E. Tompson, P. R. Aron, B. S. Chandrasekhar, and D. N. Langenberg, Phys. Rev. B 4, 518 (1971).